Red-Shifted Delayed Fluorescence at the Expense of Photoluminescence Quantum Efficiency – An Intramolecular Charge-Transfer Molecule Based on a Benzodithiophene-4,8-dione Acceptor

Stephanie Montanaro,[a] **Alexander J. Gillett**,[b] **Sascha Feldmann**,[b] **Emrys W. Evans**,[b] **Felix Plasser**,[a] **Richard H. Friend**,[b]* **and Iain A. Wright**[a]*

a Department of Chemistry, Loughborough University, Loughborough, Leicestershire, LE11 3TU, U.K.

b Optoelectronics Group, Cavendish Laboratory, University of Cambridge, Cambridge, CB3 0HE, U.K.

Abstract

Employing the thiophene based quinone, benzo[1,2-*b*:4,5-*b*']dithiophene-4,8-dione, as the electron-accepting moiety alongside *N*-phenylcarbazole donors to produce a donor-π-acceptor-π-donor (D-π-A-π-D) molecule has yielded a new red emitter displaying delayed fluorescence. This new molecule shows strongly (over 100 nm) red-shifted emission when compared to an anthraquinone based analogue. Cyclic voltammetry complemented by computational insights prove that this red-shift is due to the significantly stronger electron-accepting ability of the thiophene quinone compared to anthraquinone. Photophysical and computational studies of this molecule have revealed that while the presence of the thiophene containing acceptor facilitates rapid intersystem crossing which is comparable to anthraquinone analogues, the reverse intersystem crossing rate is slow and non-radiative decay is rapid which we can attribute to low-lying locally excited states. This limits the total photoluminescence quantum efficiency to less than 10% in both solution and the solid state. These results provide a useful example of how very minor structural variations can have a defining impact on the photophysical properties of new molecular materials.

Introduction

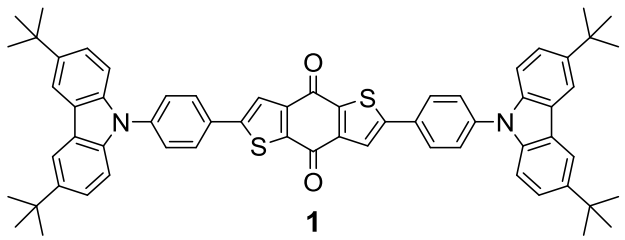

1

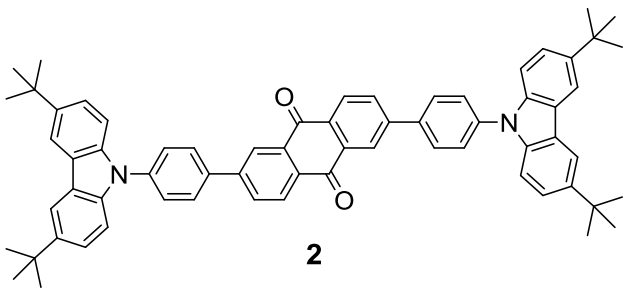

2

Benzo[1,2-*b*:4,5-*b'*]dithiophene-4,8-dione is a heterocyclic homologue of anthraquinone, featuring two thiophene rings *ortho*-fused to an electron poor 1,4-benzoquinone core, this gives it moderately strong electron accepting properties.[1,2] It is most frequently encountered as an intermediate in the synthesis of ladder-type molecules[3–11] and high performance polymers[12–20] for organic solar cells (OSCs), while its electrochemical properties have been exploited in the development of organic batteries.[21–24]

Efficient red thermally activated delayed fluorescence (TADF) is challenging due to the difficulty in simultaneously obtaining both a narrow singlet-triplet gap (ΔE_{ST}) and a high fluorescence rate constant, and in overcoming the energy gap law which predicts that as the energy gap between the ground and excited states decreases, the rate of non-radiative decay (NRD) will increase.[25–28] Anthraquinone has been employed in some of the most efficient red TADF materials[29,30] however, electrochemical studies indicate that the thiophene containing analogue benzo[1,2-*b*:4,5-*b'*]dithiophene-4,8-dione has a significantly deeper LUMO energy (ca. 0.39 V) than anthraquinone[1,31] which should give rise to red shifted optical properties. The introduction of heavy sulfur atoms may also have an impact on photophysical properties.

Therefore with the aim of producing deeper red emission arising from delayed fluorescence we decided to employ this moiety between two 3,6-di-*tert*-butyl-9*H*-carbazole electron donors separated with 1,4-phenylene spacers to produce a D-π-A-π-D type system. Here we present the synthesis and electrochemical and photophysical properties of this new molecule **1** alongside theoretical insights and some comparison with the analogous anthraquinone based molecule **2**.[29]

Synthesis

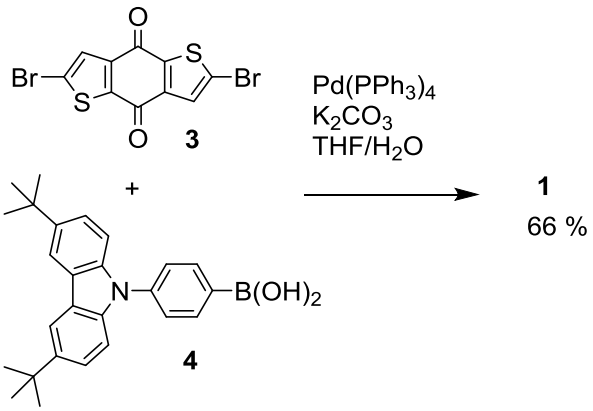

Scheme 1 Synthesis of compound **1**

Compound **1** was prepared by two-fold palladium-catalysed Suzuki coupling reaction between 2,6-dibromobenzo[1,2-*b*:4,5-*b'*]dithiophene-4,8-dione **3**[32] and (4-(3,6-di-*tert*-butyl-9*H*-carbazol-9-yl)phenyl)boronic acid **4**.[33,34] The progress of the reaction could easily be observed as the red product precipitated from the reaction mixture. After recrystallisation from *N*,*N*-dimethylformamide (DMF) **1** was obtained in 66% yield as very small, poorly soluble, purple crystals.

Thermal gravimetric analysis (TGA) demonstrated the very high thermal stability of **1** (Figure S1) which displayed an initial 2% weight drop at 133 °C arising from the loss of residual solvent of crystallisation then no further changes until total decomposition shown by a 95% weight loss at 442 °C. Prior to obtaining the TGA, we attempted to obtain a melting point and observed that the crystals display interesting solid state emission characteristics reminiscent of aggregation induced emission upon heating. As isolated, the crystals are non-emissive but when a sample of recrystallised **1** was heated to 300 °C in an open glass capillary it underwent a thermally irreversible colour change from purple to red and the crystals were now red luminescent under UV light. This seems to be related to the loss of the residual solvent as observed in the TGA measurement.

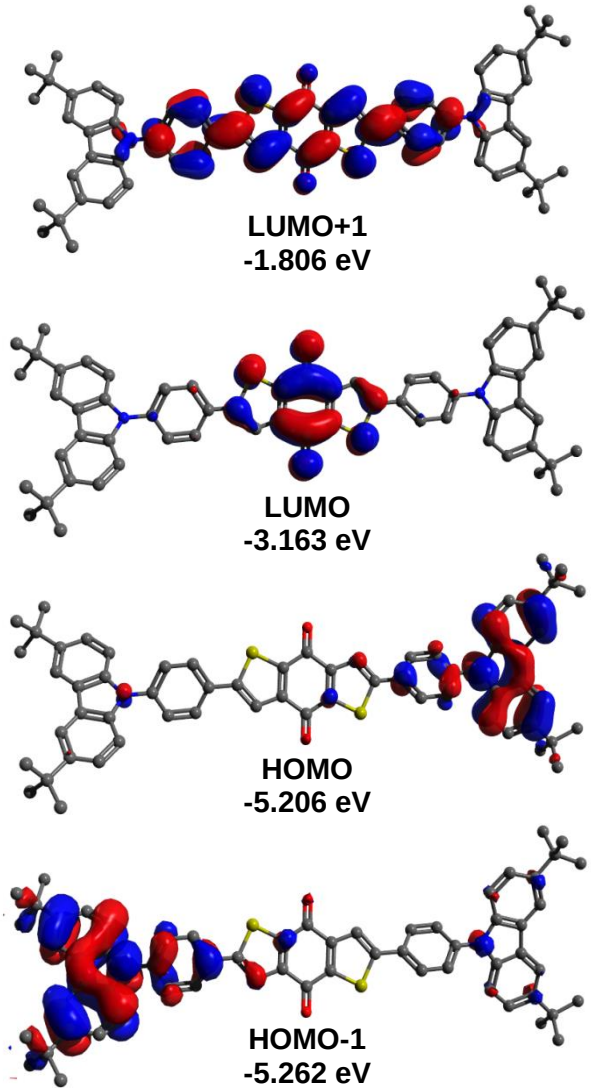

Fig. 1 Frontier orbitals of compound **1.**

Density functional theory (DFT) was used to optimise the ground state structure of **1** in toluene and the frontier orbitals were calculated using ORCA[35] employing the B3LYP functional and 6-31G* basis set (Fig. 1). This revealed the HOMO and HOMO–1 as nearly isoenergetic and residing almost exclusively over the separate 9-phenylcarbazole moieties. While the calculated bond length (1.415 Å) and dihedral angle (50°) of the carbazole–phenyl

bond are almost identical to those calculated for **2** (1.412 Å and 50° respectively), the dihedral angle of the thiophene–phenyl bond is 24° and the bond length is 1.47 Å which is comparable to those observed experimentally in the X-ray molecular structure of 2-phenylthiophene[36] and 12° more planar than the calculated anthraquinone–phenyl bond angle of 36° in **2**. Despite the increased planarity across the electron accepting core, there is little orbital overlap between the HOMO and LUMO with the LUMO distributed solely over the central dithiophene-4,8-dione core although the LUMO+1 extends across both the core and the adjacent phenyl rings.

Electrochemistry

Cyclic voltammetry (CV) was performed on a solution of **1** (Fig. 2 and Table 1) in 1,2-dichlorobenzene using a glassy carbon disc working electrode, $Ag/AgNO_3$ reference electrode and platinum wire counter electrode with 0.10 M *n*-Bu_4NPF_6 as supporting electrolyte. Reduction potentials are quoted with respect to the $E_{1/2}$ of ferrocene as internal reference.

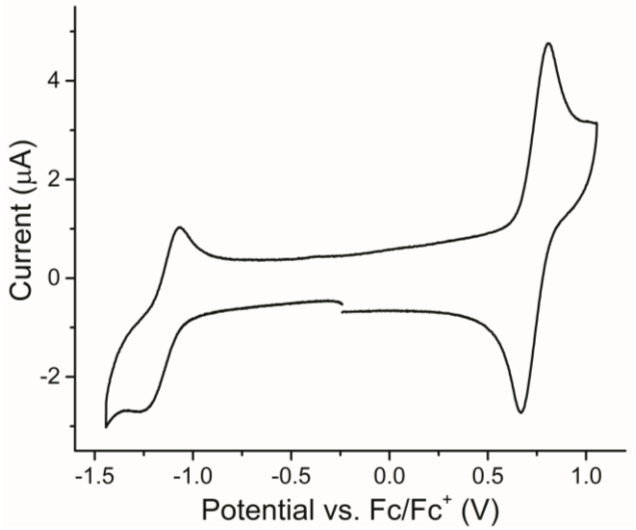

Fig. 2 Cyclic voltammetry for compound **1**.

The molecule displays a quasi-reversible (ΔE_p = 130 mV) single electron reduction of the acceptor at E_{red} = –1.15 V which is comparable to reported values for unsubstituted benzo[1,2-*b*:4,5-*b'*]dithiophene-4,8-dione[1,2] and a carbazole based reversible oxidation at E_{ox} = +0.74 V (ΔE_p = 161 mV). The magnitude of the oxidative current is significantly larger (I_p = 4.69 μA vs 2.83 μA) than that of the reduction. This implies that the wave is actually composed of two closely overlapping single electron oxidations of the two carbazole rings such that the individual waves cannot be resolved.[37] This is supported by the near-degeneracy and minimal overlap between the HOMO and HOMO–1 predicted by the DFT. Similar behaviour has also been observed in A-D-D-A type systems based upon phenothiazine dimers bearing pendant 6-hexyl-2-phenylquinolines as acceptors[38] and other π-bridged bis(triarylamine)[39–41] and bis(carbazole)[42,43] systems.

Table 1 Electrochemical properties of compound **1**

	E_{ox} (V)	E_{red} (V)	HOMO[a] (eV)	LUMO[a] (eV)	E_g[b] (eV)
1	+0.74	–1.15	-5.69	-4.10	1.59

[a]HOMO and LUMO levels estimated from the onset of the first oxidation and reduction waves respectively and are referenced the HOMO of ferrocene at –5.10 eV.
[b]Electrochemical HOMO–LUMO gap.

Photophysics

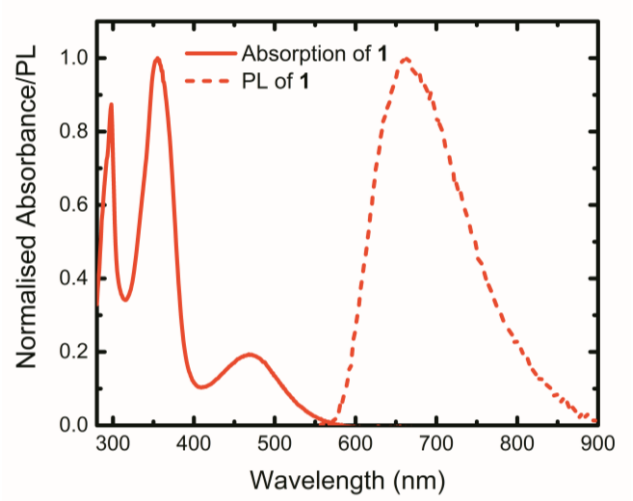

Fig. 3 The steady-state absorption and photoluminescence (PL) spectra of **1**. The measurements were performed on solutions of **1** in toluene (0.2 mg/mL for absorption and 0.5 mg/mL for PL). The excitation wavelength used for the PL was λ_{ex} = 520 nm.

An extensive photophysical characterisation of **1** has been performed, the results of which are summarized in Table 2.

Table 2 Photophysical properties of compound **1** highlighting total (Φ) and prompt (Φ_F) fluorescent PL quantum efficiency.

	$\lambda_{abs,max}$ (nm)	$\lambda_{em,max}$ (nm)	E_g[a] (eV)	Φ (soln.)	Φ_F (soln.)	Φ (film)	Φ_F (film)
1	298, 355, 468	664[b]	2.14	0.095[b]	0.084[b]	0.085[b]	0.064[b]
2[29]	426	558[c]	2.43	0.60[c]	0.43[c]	0.65[d]	0.12[d]

[a]Optical energy gap calculated from the onset of the lowest energy absorbance. [b]Excitation wavelength λ_{ex} = 520 nm. [c] Excitation wavelength λ_{ex} = 420 nm. [d]1 wt% **2** in CBP film

First examining the steady-state absorption and photoluminescence (PL) of **1** in Fig. 3, the molecule displays a low energy absorbance at 468 nm which is assigned to the computed S_2 state (Table S1) which is an intramolecular charge transfer state (ICT) between the carbazole donors and the LUMO on the dione acceptor. This ICT also corresponds to a red emission at 664 nm. We note a significant red-shift in the absorption maximum of the ICT band from 426 nm to 468 nm and a corresponding red-shift in the PL maximum from 558 nm to 664 nm when compared to **2**.[29] This effect can be directly attributed to the use of the stronger electron accepting benzo[1,2-*b*:4,5-*b'*]dithiophene-4,8-dione moiety, which leads to a significant drop in the position of the LUMO and a reduced optical band gap of 2.14 eV. However, the PL quantum efficiency (PLQE) of **1** was much lower than **2**, displaying values of 9.5% for a 0.5 mg/mL solution in oxygen-free toluene and 8.4% in non-degassed toluene compared to 60% and 43% respectively for **2**. A 2 wt % film of **1** doped in polystyrene and encapsulated in an N_2 atmosphere displayed a total PLQE of only 8.5%.

To examine the reasons behind the low PLQE value, we first performed transient absorption (TA) spectroscopy on a film of 2 wt% **1** doped into polystyrene. In the short-time (100 fs – 1.6 ns) TA (Figure S2), we observe the formation of two new photo induced absorption (PIA) bands: one at 575 nm and the other in the near-infrared (NIR) at 1000 nm. In this initial short time range, we do not observe any spectral evolution of the PIAs, but the band at 575 nm seems to decay marginally more quickly than the 1000 nm feature falling to approximately 70% of its original intensity, compared to 80% for the NIR PIA.

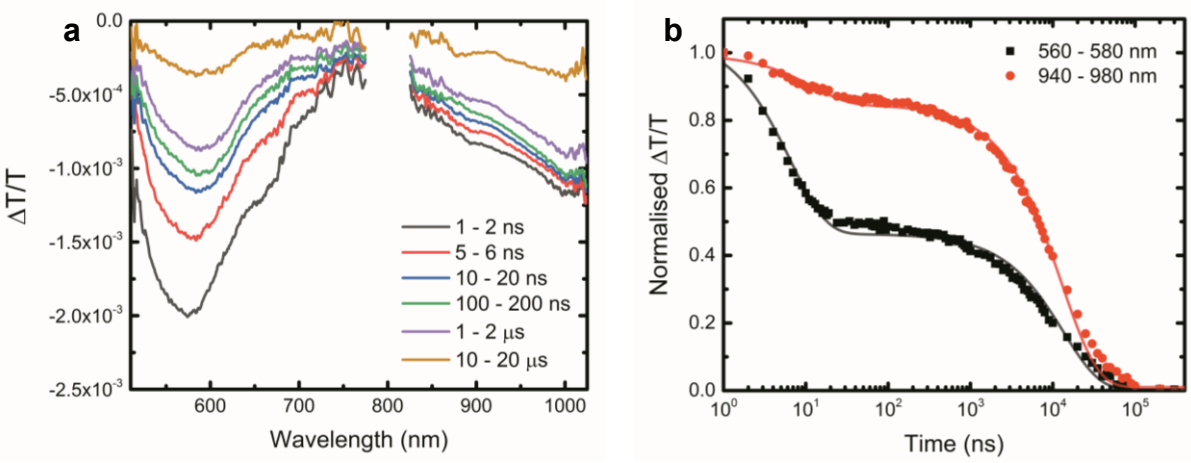

Fig. 4 a Long time TA spectrum of a film of **1** doped at 2 wt % in polystyrene, taken at different time points. The film was excited at λ_{ex} = 355 nm, with a fluence of 28 μJ/cm^2. **b** The normalised kinetics taken from the wavelength regions of 560 – 580 nm and 940 – 980 nm. Both kinetics were fitted with bi-exponential decay functions, which are represented as the solid lines. The fits yielded time constants of τ_{prompt} = 6.6 ns, $\tau_{delayed}$ = 13.6 μs and τ_{prompt} = 12.0 ns, $\tau_{delayed}$ = 12.8 μs for the 560 – 580 nm and 940 – 980 nm regions, respectively.

Turning to the long timescale TA (1 ns – 400 μs) in Fig.4, we again observe the same two bands as in the short timescale TA. Both bands display bi-exponential decay kinetics which is typical of TADF behaviour.[44] This suggests an initial radiative or non-radiative loss of singlet excited states to the ground state alongside forward intersystem crossing (ISC) of the remaining singlet population to the triplet manifold, prior to the delayed decay of S_1 states which have formed by repopulation through reverse intersystem crossing (rISC). The band at

575 nm shows an initial prompt decay, presumably due to relaxation from S_1 to S_0, which is more rapid than that of the 1000 nm band with over 50% of excited state species lost after approximately 10 ns. This is followed by the much slower delayed component. This assumes no significant change in oscillator strength between the species present at early and late timescales. The decay kinetics yielded time constants of τ_{prompt} = 6.6 ns, $\tau_{delayed}$ = 13.6 μs and τ_{prompt} = 12.0 ns, $\tau_{delayed}$ = 12.8 μs for the 560 – 580 nm and 940 – 980 nm regions, respectively. The position, rate of decay and diminished prompt component of the long wavelength PIA indicates that a significant proportion of the species responsible for this band undergo ISC much faster than decay to S_0. Therefore it may be assigned primarily to excitation of T_1 to higher triplet states. An alternative explanation for discrepancies in the decay rates for the two PIAs could be the presence of multiple conformers with different intrinsic decay and ISC rates, as has been previously observed in organic D-A-D type TADF compounds.[45,46] Considering these results, we suggest that the PIA at 575 nm is responsible for the majority of the prompt fluorescence.

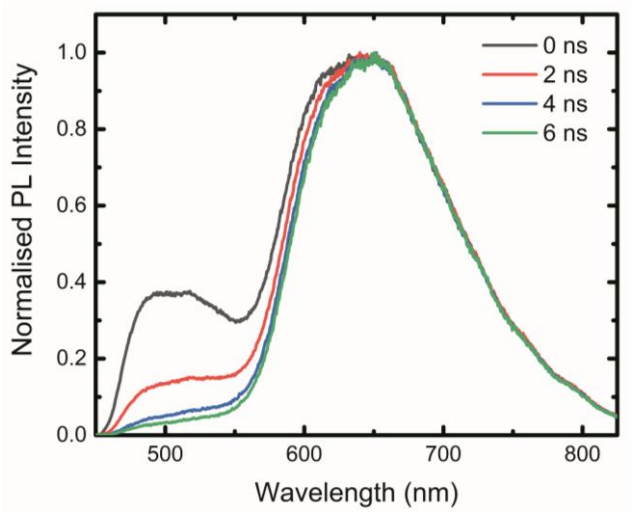

Fig. 5 Early time spectral slices of **1** doped at 2 wt % in polystyrene. The film was excited at λ_{ex} = 400 nm, with a fluence of 176 μJ/cm^2. Clearly visible is a new PL band peaked around 520 nm that decays with a time constant faster than the instrument response of the setup.

When observing the ns-ms transient PL (trPL) of **1**, a new PL band in addition to the primary ICT emission is observed at 520 nm that decays with a time constant shorter that the instrument response of our setup of ~2 ns (Fig. 5). Similar high energy bands have been observed for a number of TADF systems and typically arise from the presence of different molecular conformations.[47–49] Ultrafast transient grating PL studies on the film with an excitation wavelength of 400 nm reveal that this emission is present from the earliest timescales detectable of 200 fs and is almost completely decayed by 1 ns (Figure S3). Interestingly, this band is visible in the steady-state PL of the film when excited at 405 nm, but not when the excitation wavelength is 520 nm (Figure S4). Tellingly, this band is also not visible in the steady-state PL of **1** in a toluene solution when excited at 405 nm (Figure S5), ruling out emission from a high energy local excited singlet state. We know that in the solid-state, many different rotational conformers can exist in tandem, locked-in by the high energetic barrier to rotation.[45] This is in contrast to solution, where the additional rotational freedom lowers this barrier and allows for the rapid interconversion between conformers,

leading to an equilibrium between states that strongly favours the lower energy conformers. Important to note is that each of these stable conformers possesses their own distinct band gap,[50] leading to the presence of many different species with unique band gaps in the film. Therefore, we assign this short-lived green PL to the emission from higher energy conformers, only excited by the blue pump photons. The short, sub-ns lifetime of this emission is due to rapid energy transfer from these conformers to their lower band gap neighbours in the film, which quenches the green emission.

Focussing on the primary ICT emission, we track the kinetics from the emission peak between 640 – 660 nm and integrate the resulting trace (Fig 6). From this, we determine that 98% of the total PL emission occurs within the first 40 ns. The trPL decay kinetics are not readily fitted by a simple bi-exponential decay, likely due to the convolution of decays from multiple conformers. But the timescales for the decay processes appear to be broadly in-line with those observed in the TA. By combining this information with the insight gained from the TA, it is immediately apparent why the PLQE of **1** is relatively low: a significant proportion of the excited states that enter the triplet manifold do not undergo rISC and ultimately decay non-radiatively.

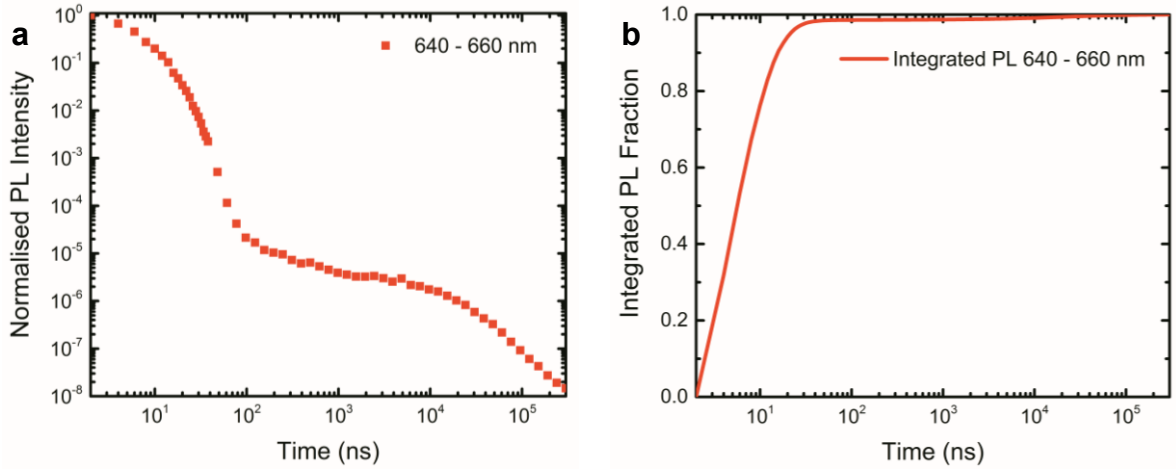

Fig. 6 a The normalised PL decay kinetic of **1** doped at 2 wt % in polystyrene. The film was excited at λ_{ex} = 400 nm, with a fluence of 176 μJ/cm^2. The kinetics displayed were averaged from the wavelength regions of 640 – 660 nm, corresponding to the PL maximum. **b** The integrated PL decay kinetics from the 640 – 660 nm region, showing that 98% of the total PL has been emitted by 40 ns.

Revisiting the PL and TA results for the doped film and focussing on the band at 575 nm, calculation of the rate constant for: i) the prompt radiative decay of the singlet states, k_r^S = 9.73×10^6 s^{-1}; ii) intersystem crossing, k_{ISC} = 1.42×10^8 s^{-1}; iii) reverse intersystem crossing, k_{RISC} = 2.58×10^4 s^{-1}; iv) the non-radiative decay of the triplet state k_{nr}^T = 7.18×10^4 s^{-1}, [51,52] (using equations S1-S4) indicates that non-radiative decay of the triplet state is occurring significantly more rapidly than any rISC. Similar calculations performed after photophysical studies of a molecule related to **2** (doped into zeonex at 2 wt %) which features an anthraquinone core bearing diphenylamine donors,[46] revealed that the k_r^S of **1** is an order of magnitude slower while the k_{RISC} of **1** was two orders of magnitude slower. Conversely, the k_{nr}^T of **1** is faster. The calculated values for k_{ISC} are comparable.

While, in accordance with the energy gap law, we may expect the rate of NRD to increase with decreasing emission energy, the use of the thiophene acceptor has resulted in an 85% decrease in PLQE when comparing **1** and **2** which seems particularly stark. While conformational relaxation of T_1 can facilitate non-radiative decay[46] another possible explanation for both the drop in k_r^S and the acceleration of k_{nr}^T is that strong spin–orbit coupling from the heavy sulfur atoms facilitates efficient ISC before low lying triplet states of the thiophene rings mediate NRD from T_1 to S_0.[53–55] Revisiting our computational results we performed time-dependent DFT experiments to obtain a deeper picture of the electronic structure of the molecule. The results of the calculations (Table S1) showed a good agreement with our experimental results. A computed ΔE_{ST} of 0.54 eV was obtained while the calculations also revealed that the T_1 state of **1** is a low-energy local excitation on the benzodithiophene unit located at 1.95 eV, which is 0.77 eV lower than the bright S_2 state. In total there are four triplet and one singlet state below S_2 and we suggest that this high density of dark low energy states is severely inhibiting rISC and therefore limiting delayed fluorescence.

Conclusions

We have confirmed that the use of electron deficient benzo[1,2-*b*:4,5-*b'*]dithiophene-4,8-dione in a D-π-A-π-D type molecule results in an emission red-shift of over 100 nm in solution while maintaining long-lived excited states when compared to an analogous anthraquinone based emitter. Through a detailed photophysical and computational study, we have determined that this red-shift in emission occurs at the expense of the PLQE due to the presence of low-energy local singlet and triplet states on the benzodithiophene, diminished rISC and rapid NRD. As the presence of heavy sulfur atoms and low-lying triplet energies in thiophene facilitates this rapid NRD then employing the comparably electron deficient[2] but heavy atom free furan analogue, benzo[1,2-*b*:4,5-*b'*]difuran-4,8-dione, presents an interesting avenue to explore.

Conflicts of Interest

There are no conflicts of interest to declare.

Acknowledgements

I.A.W. thanks Loughborough University for support and the Royal Society of Chemistry Research Fund (RF18-5353) for funding. I.A.W. also thanks the Durham University Mass Spectrometry Service for ASAP-MS. S.M. acknowledges Loughborough University for providing a PhD studentship. A.J.G and R.H.F. thank the EPSRC for support. S.F. acknowledges funding from the Studienstiftung des deutschen Volkes and the EPSRC. Sandra Dressler is thanked for running TGA analysis.

Supplementary Information Available: Synthesis and characterisation of **1** and the experimental details for the computational, electrochemical and photophysical studies are provided in the supporting information.

References

1 K. Kobayashi and K. Umemoto, *Bull. Chem. Soc. Jpn.*, 1992, **65**, 2168–2172.

2 M. Büschel, C. Stadler, C. Lambert, M. Beck and J. Daub, *J. Electroanal. Chem.*, 2000, **484**, 24–32.

3 S. Fu, X. Zhu, G. Zhou, W. Y. Wong, C. Ye, W. K. Wong and Z. Li, *Eur. J. Inorg. Chem.*, 2007, **2007**, 2004–2013.

4 Y. J. Kim, J. Y. Baek, J. J. Ha, D. S. Chung, S. K. Kwon, C. E. Park and Y. H. Kim, *J. Mater. Chem. C*, 2014, **2**, 4937–4946.

5 B. Kan, Q. Zhang, F. Liu, X. Wan, Y. Wang, W. Ni, X. Yang, M. Zhang, H. Zhang, T. P. Russell and Y. Chen, *Chem. Mater.*, 2015, **27**, 8414–8423.

6 Y. Z. Lin, C. W. Yeh, P. T. Chou, M. Watanabe, Y. H. Chang, Y. J. Chang and T. J. Chow, *Dye. Pigment.*, 2014, **109**, 81–89.

7 Y. Lin, J. Wang, Z. G. Zhang, H. Bai, Y. Li, D. Zhu and X. Zhan, *Adv. Mater.*, 2015, **27**, 1170–1174.

8 W. He, M. Y. Livshits, D. A. Dickie, J. Yang, R. Quinnett, J. J. Rack, Q. Wu and Y. Qin, *Chem. Sci.*, 2016, **7**, 5798–5804.

9 T. J. Aldrich, M. J. Leonardi, A. S. Dudnik, N. D. Eastham, B. Harutyunyan, T. J. Fauvell, E. F. Manley, N. Zhou, M. R. Butler, T. Harschneck, M. A. Ratner, L. X. Chen, M. J. Bedzyk, R. P. H. Chang, F. S. Melkonyan, A. Facchetti and T. J. Marks, *ACS Energy Lett.*, 2017, **2**, 2415–2421.

10 Y. Li, L. Zhong, B. Gautam, H. J. Bin, J. D. Lin, F. P. Wu, Z. Zhang, Z. Q. Jiang, Z. G. Zhang, K. Gundogdu, Y. Li and L. S. Liao, *Energy Environ. Sci.*, 2017, **10**, 1610–1620.

11 Q. Liu, Z. Xiao, T. Li, S. Yang, W. You, M. Wang and L. Ding, *Mater. Chem. Front.*, 2018, **2**, 1563–1567.

12 J. Hou, M. H. Park, S. Zhang, Y. Yao, L. M. Chen, J. H. Li and Yang, *Macromolecules*, 2008, **41**, 6012–6018.

13 Y. Liang, D. Feng, Y. Wu, S. T. Tsai, G. Li, C. Ray and L. Yu, *J. Am. Chem. Soc.*, 2009, **131**, 7792–7799.

14 H. Y. Chen, J. Hou, S. Zhang, Y. Liang, G. Yang, Y. Yang, L. Yu, Y. Wu and G. Li, *Nat. Photonics*, 2009, **3**, 649–653.

15 Y. Liang, Z. Xu, J. Xia, S. T. Tsai, Y. Wu, G. Li, C. Ray and L. Yu, *Adv. Mater.*, 2010, **22**, E135–E138.

16 M. L. Keshtov, G. D. Sharma, V. S. Kochurov and A. R. Khokhlov, *Synth. Met.*, 2013, **166**, 7–13.

17 T. Qin, W. Zajaczkowski, W. Pisula, M. Baumgarten, M. Chen, M. Gao, G. Wilson, C. D. Easton, K. Müllen and S. E. Watkins, *J. Am. Chem. Soc.*, 2014, **136**, 6049–6055.

18 H.-C. Liao, T. L. D. Tam, P. Guo, Y. Wu, E. F. Manley, W. Huang, N. Zhou, C. M. M. Soe, B. Wang, M. R. Wasielewski, L. X. Chen, M. G. Kanatzidis, A. Facchetti, R. P. H. Chang and T. J. Marks, *Adv. Energy Mater.*, 2016, **6**, 1600502.

19 S. Chen, Y. Liu, L. Zhang, P. C. Y. Chow, Z. Wang, G. Zhang, W. Ma and H. Yan, *J. Am. Chem. Soc.*, 2017, **139**, 6298–6301.

20 H. Huang, H. Bin, Z. Peng, B. Qiu, C. Sun, A. Liebman-Pelaez, Z.-G. Zhang, C. Zhu, H. Ade, Z. Zhang and Y. Li, *Macromolecules*, 2018, **51**, 6028–6036.

21 B. Häupler, T. Hagemann, C. Friebe, A. Wild and U. S. Schubert, *ACS Appl. Mater. Interfaces*, 2015, **7**, 3473–3479.

22 S. D. Pineda Flores, G. C. Martin-Noble, R. L. Phillips and J. Schrier, *J. Phys. Chem. C*, 2015, **119**, 21800–21809.

23 X. Chen, Y. Wu, Z. Huang, X. Yang, W. Li, L. C. Yu, R. Zeng, Y. Luo and S. L. Chou, *J. Mater. Chem. A*, 2016, **4**, 18409–18415.

24 Y. Jing, Y. Liang, S. Gheytani and Y. Yao, *Nano Energy*, 2017, **37**, 46–52.

25 J. H. Kim, J. H. Yun and J. Y. Lee, *Adv. Opt. Mater.*, 2018, **6**, 1800255.

26 L. Gan, X. Li, X. Cai, K. Liu, W. Li and S. J. Su, *Beilstein J. Org. Chem.*, 2018, **14**, 672–681.

27 J. X. Chen, K. Wang, C. J. Zheng, M. Zhang, Y. Z. Shi, S. L. Tao, H. Lin, W. Liu, W. W. Tao, X. M. Ou and X. H. Zhang, *Adv. Sci.*, 2018, **5**, 1800436.

28 R. Furue, K. Matsuo, Y. Ashikari, H. Ooka, N. Amanokura and T. Yasuda, *Adv. Opt. Mater.*, 2018, **6**, 1701147.

29 Q. Zhang, H. Kuwabara, W. J. Potscavage, S. Huang, Y. Hatae, T. Shibata and C. Adachi, *J. Am. Chem. Soc.*, 2014, **136**, 18070–18081.

30 K. Sun, D. Chu, Y. Cui, W. Tian, Y. Sun and W. Jiang, *Org. Electron.*, 2017, **48**, 389–396.

31 S. Yamaguchi, H. Tatemitsu, Y. Sakata and S. Misumi, *Chem. Lett.*, 1983, **12**, 1229–1230.

32 C. Y. Kuo, W. Nie, H. Tsai, H. J. Yen, A. D. Mohite, G. Gupta, A. M. Dattelbaum, D. J. William, K. C. Cha, Y. Yang, L. Wang and H. L. Wang, *Macromolecules*, 2014, **47**, 1008–1020.

33 E. Ishow, R. Camacho-Aguilera, J. Guérin, A. Brosseau and K. Nakatani, *Adv. Funct. Mater.*, 2009, **19**, 796–804.

34 W. Sun, N. Zhou, Y. Xiao, S. Wang and X. Li, *Dye. Pigment.*, 2018, **154**, 30–37.

35 F. Neese, *Wiley Interdiscip. Rev. Comput. Mol. Sci.*, 2012, **2**, 73–78.

36 S. Lois, J. C. Florès, J. P. Lère-Porte, F. Serein-Spirau, J. J. E. Moreau, K. Miqueu, J. M. Sotiropoulos, P. Baylère, M. Tillard and C. Belin, *European J. Org. Chem.*, 2007, **2007**, 4019–4031.

37 R. F. Winter, *Organometallics*, 2014, **33**, 4517–4536.

38 R. Y. Lai, X. Kong, S. A. Jenekhe and A. J. Bard, *J. Am. Chem. Soc.*, 2003, **125**, 12631–12639.

39 S. Barlow, C. Risko, S. A. Odom, S. Zheng, V. Coropceanu, L. Beverina, J. L. Brédas and S. R. Marder, *J. Am. Chem. Soc.*, 2012, **134**, 10146–10155.

40 S. Barlow, C. Risko, S. J. Chung, N. M. Tucker, V. Coropceanu, S. C. Jones, Z. Levi, J. L. Brédas and S. R. Marder, *J. Am. Chem. Soc.*, 2005, **127**, 16900–16911.

41 S. Zheng, S. Barlow, C. Risko, T. L. Kinnibrugh, V. N. Khrustalev, S. C. Jones, M. Y. Antipin, N. M. Tucker, T. V. Timofeeva, V. Coropceanu, J. L. Brédas and S. R. Marder, *J. Am. Chem. Soc.*, 2006, **128**, 1812–1817.

42 S. Kato, H. Noguchi, A. Kobayashi, T. Yoshihara, S. Tobita and Y. Nakamura, *J. Org. Chem.*, 2012, **77**, 9120–9133.

43 I. A. Wright, H. A. Al-Attar, A. S. Batsanov, A. P. Monkman and M. R. Bryce, *Phys. Chem. Chem. Phys.*, 2018, **20**, 11867–11875.

44 H. Uoyama, K. Goushi, K. Shizu, H. Nomura and C. Adachi, *Nature*, 2012, **492**, 234–238.

45 J. S. Ward, R. S. Nobuyasu, M. A. Fox, A. S. Batsanov, J. Santos, F. B. Dias and M. R. Bryce, *J. Org. Chem.*, 2018, **83**, 14431–14442.

46 Z. Kuang, G. He, H. Song, X. Wang, Z. Hu, H. Sun, Y. Wan, Q. Guo and A. Xia, *J. Phys. Chem. C*, 2018, **122**, 3727–3737.

47 P. L. Dos Santos, M. K. Etherington and A. P. Monkman, *J. Mater. Chem. C*, 2018, **6**, 4842–4853.

48 N. Acar, J. Kurzawa, N. Fritz, A. Stockmann, C. Roman, S. Schneider and T. Clark, *J. Phys. Chem. A*, 2003, **107**, 9530–9541.

49 N. A. Kukhta, A. S. Batsanov, M. R. Bryce and A. P. Monkman, *J. Phys. Chem. C*, 2018, **122**, 28564–28575.

50 M. Okazaki, Y. Takeda, P. Data, P. Pander, H. Higginbotham, A. P. Monkman and S. Minakata, *Chem. Sci.*, 2017, **8**, 2677–2686.

51 K. Goushi, K. Yoshida, K. Sato and C. Adachi, *Nat. Photonics*, 2012, **6**, 253–258.

52 K. Masui, H. Nakanotani and C. Adachi, *Org. Electron.*, 2013, **14**, 2721–2726.

53 S. C. Rasmussen, S. J. Evenson and C. B. McCausland, *Chem. Commun.*, 2015, **51**, 4528–4543.

54 R. S. Becker, J. Seixas de Melo, A. L. Maçanita and F. Elisei, *J. Phys. Chem.*, 1996, **100**, 18683–18695.

55 S. Rentsch, J. P. Yang, W. Paa, E. Birckner, J. Schiedt and R. Weinkauf, *Phys. Chem. Chem. Phys.*, 1999, **1**, 1707–1714.